

Computed reconstruction of spatial ammonoid-shell orientation captured from digitized grinding and landmark data



Susanne Lukeneder^{a,*}, Alexander Lukeneder^a, Gerhard W. Weber^b

^a Natural History Museum Vienna, Geological-Paleontological Department, Burgring 7, A-1010 Vienna, Austria

^b Department of Anthropology, University of Vienna, Althanstraße 14, A-1090 Vienna, Austria

ARTICLE INFO

Article history:

Received 6 August 2013

Received in revised form

16 November 2013

Accepted 21 November 2013

Available online 12 December 2013

Keywords:

Spatial shell orientation

Destructive 3D-visualization

Amira 3D-software

Triassic ammonoids

Mass occurrences

Stereographic analyses

ABSTRACT

The internal orientation of fossil mass occurrences can be exploited as useful source of information about their primary depositional conditions. A series of studies, using different kinds of fossils, especially those with elongated shape (e.g., elongated gastropods), deal with their orientation and the subsequent reconstruction of the depositional conditions (e.g., paleocurrents and transport mechanisms). However, disk-shaped fossils like planispiral cephalopods or gastropods were used, up to now, with caution for interpreting paleocurrents. Moreover, most studies just deal with the topmost surface of such mass occurrences, due to the easier accessibility. Within this study, a new method for three-dimensional reconstruction of the internal structure of a fossil mass occurrence and the subsequent calculation of its spatial shell orientation is established. A 234 million-years-old (Carnian, Triassic) monospecific mass occurrence of the ammonoid *Kasimlarceltis krystyni* from the Taurus Mountains in Turkey, embedded in limestone, is used for this pilot study. Therefore, a 150 × 45 × 140 mm³ block of the ammonoid bearing limestone bed has been grinded to 70 slices, with a distance of 2 mm between each slice. By using a semi-automatic region growing algorithm of the 3D-visualization software Amira, ammonoids of a part of this mass occurrence were segmented and a 3D-model reconstructed. Landmarks, trigonometric and vector-based calculations were used to compute the diameters and the spatial orientation of each ammonoid. The spatial shell orientation was characterized by dip and dip-direction and aperture direction of the longitudinal axis, as well as by dip and azimuth of an imaginary sagittal-plane through each ammonoid. The exact spatial shell orientation was determined for a sample of 675 ammonoids, and their statistical orientation analyzed (i.e., NW/SE). The study combines classical orientation analysis with modern 3D-visualization techniques, and establishes a novel spatial orientation analyzing method, which can be adapted to any kind of abundant solid matter.

© 2013 The Authors. Published by Elsevier Ltd. Open access under CC BY-NC-ND license.

1. Introduction

1.1. Mass occurrences and their internal orientation as key to paleoenvironments

Abundant marine fossils, especially with elongated shapes (e.g., belemnites), are useful indicators to draw conclusions about influencing factors (e.g., sea floor paleocurrents and transport mechanisms) of paleoenvironments. Since Hall (1843) regarded the orientation of brachiopod valves as current induced, a series of studies have been conducted concerning fossil orientation

measurements (Potter and Pettijohn, 1977). Orthocone cephalopods (e.g., nautiloids like *Orthoceras*; Wendt et al., 1984; Wendt, 1995), gastropods (e.g., Seilacher, 1959, 1960; Wendt, 1995; Cataldo et al., 2013), bivalves (Kelling and Moshrif, 1977), foraminifers (King, 1948), tentaculite shells (Hladil et al., 1996), trilobites (Seilacher, 1959, 1960) and vertebrate bones (e.g. Vasićkova et al., 2012) have been used so far in field-based spatial orientation studies (Flügel, 2004). Kidwell et al. (1986) analyzed two-dimensional geometries of skeletal accumulations with focus on their preferred orientation. However, the indication of current patterns is not only restricted to fossils with elongated basic shape and their nature to be reoriented by any kind of current. Planispirally coiled (disk-shaped) forms like gastropods, but also cephalopods such as ammonoids can also provide such depositional information (e.g., Futterer, 1982; Wendt, 1995; Lukeneder, 2005; Olivero, 2007; Seilacher, 1971; Wani, 2006, 2007).

The main aim of this study is to present a novel method for analyzing spatial orientation, which can be adapted to all kinds of

* Corresponding author. Tel.: +43 1 52177 251; fax: +43 1 52177 459.
E-mail address: susanne.lukeneder@nhm-wien.ac.at (S. Lukeneder).

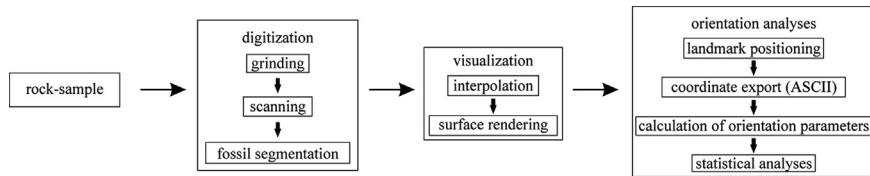


Fig. 1. Steps used for digitization and visualization of the ammonoids as well as for subsequent calculation and evaluation of their spatial shell-orientation.

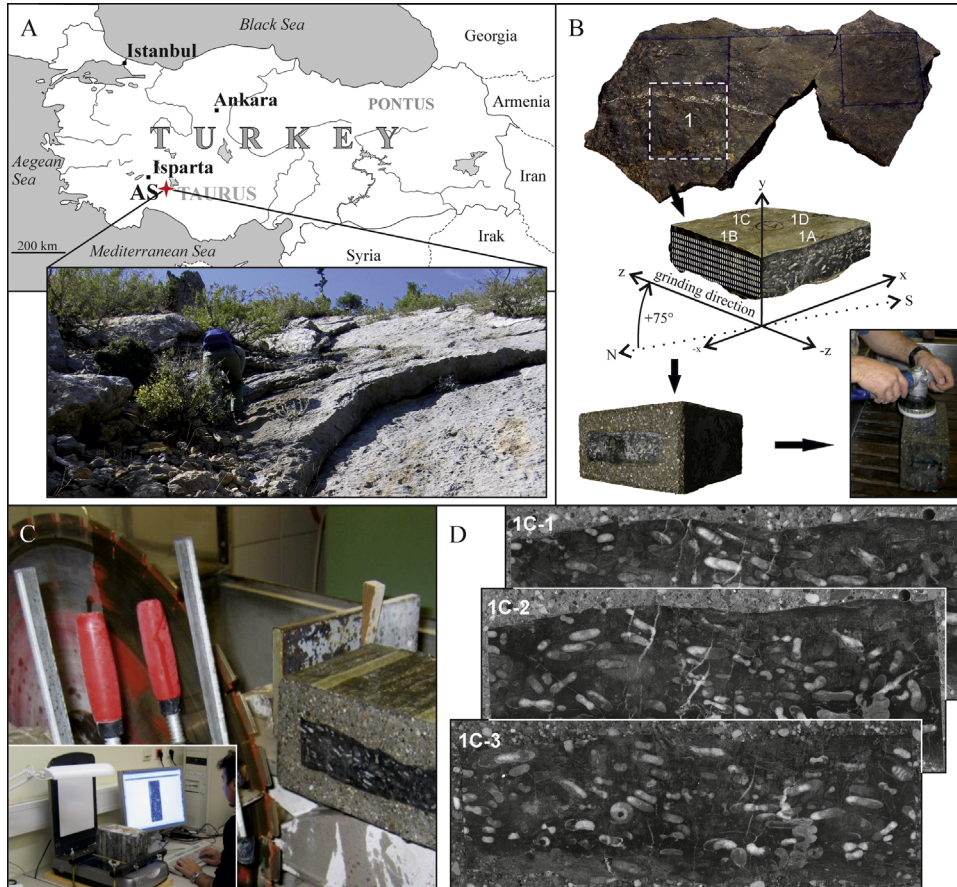


Fig. 2. Explanation of the grinding and digitizing method of the ammonoid mass occurrence from Aşağıyaylabel. (A) Geographic location of the limestone bed. (B) The recovered limestone bed and the $150 \times 45 \times 140 \text{ mm}^3$ limestone sample, which was geographically adjusted and set into concrete. (C) Grinding, polishing and scanning of the slices. (D) Three examples of the 70 scanned slices, with a distance of 2 mm.

abundant solid matter such as fossils and particles or to geological features such as faults, folds or rock core analyses.

1.2. Serial-grinding as possible alternative to computed tomography

The application of 3D-visualization on different kinds of objects and in different scientific fields has increased enormously. Since [Sollas \(1903\)](#) introduced the method of serial sectioning within his work on Therapsida and Lysorophia ([Camp and Hanna, 1937](#)), 3D-visualization has been adapted for a wide field of paleontological studies (e.g., [VanderHoof, 1931](#); [Simpson, 1933](#); [Koslowski, 1932](#); [Stensiö, 1927](#); [Fourie, 1974](#); [Conroy and Vannier, 1984](#); [Ketcham and Carlson, 2001](#); [Marschallinger, 2001, 2011](#); [Dockner, 2006](#); [Sutton, 2008](#); [Garwood et al., 2010](#); [Briguglio et al., 2011](#); [Kruta et al., 2011](#); [Lukeneder, 2012](#)). The most obvious method used for digitization today is computed tomography (CT) with all its derivatives (e.g., macro-CT, μ -CT, nano-CT, etc.). However, CT is not always successful, particularly when the density

contrast of the involved materials is too low. This is exactly the case for the herein presented ammonoid mass occurrence, caused by the almost equal density of the ammonoid shells (i.e., secondary calcite shells, $2.6\text{--}2.8 \text{ g/cm}^3$) and the embedding source rock (limestone, 2.8 g/cm^3). Therefore, we applied the classic method of serial-grinding, despite its invasive and (partially or entirely) destructive character. If samples are large enough to sacrifice fractions of it, serial grinding represents a good alternative in cases when digital recording methods fail, because in addition to a good resolution, color information (not available in CT-scans) can be obtained as well.

In our approach, we focus on the three-dimensional reconstructions of the ammonoids from the entire bed, instead of focusing on the fossil orientation on the surface of a sedimentary horizon. This and the spatial analysis of their orientation within a stereographic projection plot are the main innovations of this study compared to other conventional fossil-orientation-studies. An overview over the entire approach, from fossil collection to orientation analyses, can be gleaned from Fig. 1.

2. Paleontological material

The directional data are derived from a monospecific ($> 99\%$) ammonoid mass occurrence of *Kasimlarceiltites krystyni* (Lukeneder and Lukeneder, in press). The mass occurrence is situated within the Taurus Mountains of Turkey, at the Kasimlar Formation of the section Aşağıyaylabel, about 90 km northeast of Antalya and 70 km southeast of Isparta (WGS 84N $37^{\circ} 33' 05''$, E $31^{\circ} 18' 14''$; Fig. 2A). It is part of a limestone bed (Fig. 2A and B), deposited during the Late Triassic (234 mya) within an intrashelf-basin at the western end of the “Cimmerian terranes” (western Tethys Ocean; Şengör et al., 1984; Dercourt et al., 1993, 2000; Gindl, 2000; Scotese et al., 1989; Scotese, 1998, 2001; Stampfli and Borel, 2002; Stampfli et al., 2002; Lukeneder et al., 2012). The deposition of this mass occurrence during an important time-slice makes them suitable for investigations related to conclusions about its paleoenvironment. The reference material of this limestone bed has been collected during a field trip in 2007. The resulting raw-data-slices as well as the extant material are stored at the Natural History Museum of Vienna (NHMW-2012/0133/0480-550).

3. Methods

3.1. Serial grinding and digitization

A $150 \times 45 \times 140 \text{ mm}^3$ block was cut from the ammonoid-bearing limestone bed of Aşağıyaylabel, and for stabilization, set into concrete (Fig. 2B). For designation and the subsequent exact digital stacking of the resulting slices, two cores of 4.4 mm diameter were drilled on the lower right and the upper left edge of the block and a 1 mm iron rod inserted. By using a stone saw, the block was grinded longitudinally (from slice 1A to 1C; Fig. 2B) into 70 slices with a spacing of 2 mm (Fig. 2C). All slices were

scanned using the commercial scanning system Epson Perfection 4990 Photo. They were digitized with a resolution of 1200 dpi, and stored as 8 bit gray-scale TIFF image (Fig. 2C and D).

3.2. 3D-visualization

For the visualization of the ammonoids, two different methods of computer facilities have been tested. Manual digitization with CorelDRAW X4 and Gocad (Mayrhofer and Lukeneder, 2011; Lukeneder and Lukeneder, 2011; see Supplementary Fig. 1) has been declined after testing a more appropriate method, the semi-automatic region growing algorithm of the 3D-visualization software Amira.

3.2.1. Amira

The software package Amira is a 3D-Software for Life Sciences & Biomedical Data. 3D-volume objects can be segmented relatively fast and easily from 2D-slices using sophisticated segmentation algorithms.

- 1. Alignment of slices** – For uploading the slices into Amira, consistent physical dimensions of the pictures are needed for registration. Therefore, a template was created to standardize the pixel size and scope of all slices, after correcting the alignment of their designation-cores, using the software CorelDRAW. Each slice was aligned to the subsequent and copied onto a black rectangular template (Fig. 3A), which guarantees constant physical dimensions. The stack of scanned slices with consistent pixel size (0.254) and dimensions (1377×669 pixels) were loaded into Amira, and placed at the correct distance of grinding (2 mm) by using the bounding box tool.
- 2. Ammonoid segmentation** – While ammonoids cannot successfully be distinguished from their surrounding matrix in CT-applications, they show different gray values (Fig. 3A) in the photographed slices. Therefore, the semi-automatic region

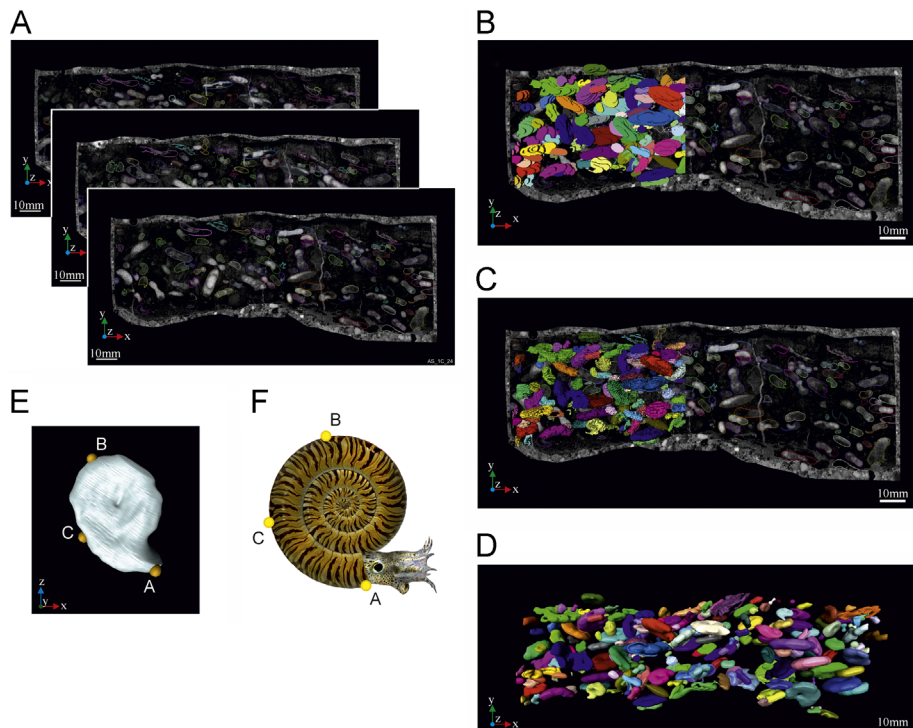


Fig. 3. Steps of the segmentation-procedure applied to the ammonoids from the scanned slices via Amira. (A) Indicated segmentation of ammonoids via semi-automatic region growing technique. (B) Lable-fields and (C) interpolated lable-fields of the segmented ammonoids. (D) Rendered ammonoid surfaces from interpolated lable-fields. (E) Positions of the landmarks, set on every ammonoid-surface. (F) Landmark positions shown at a virtual ammonoid model, designed by 7Reasons.

growing algorithm of Amira allowed a quite fast segmentation. This algorithm is based on a particular threshold gray-value, defined by the user. After setting a seed point at a suitable spot, the neighboring pixels respectively voxels will be added to an entity called label-field as long as they correspond to the defined parameters, i.e., gray-value range (Weber and Bookstein, 2011). To prevent the region growing algorithm from escaping into unwanted areas (where gray values of the matrix are too similar), limits had to be set manually at some locations (therefore we call the method “semi-automatic” instead of “automatic”). The number of these interventions was kept as minimal as possible to proceed with the segmentation. For detailed information about different segmentation techniques see Malcom and Jones (2001), Spinsby et al. (2008) as well as Weber and Bookstein (2011).

3. Surface rendering – The 2 mm space between the segmented ammonoid slices (segmented label-fields; Fig. 3B) was interpolated (interpolated label-fields; Fig. 3C). Subsequently, 3D ammonoid surfaces (triangulated isosurfaces) were rendered from the interpolated label-fields (Fig. 3D). Each ammonoid could be assigned to its own triangulated isosurface and color (Fig. 3D and E).

3.3. Orientation measurements

The basic data for computing orientation values of the ammonoids were also produced in Amira using landmarks set at each segmented ammonoid (Fig. 3E and F).

3.3.1. Landmark positioning

The first landmark (A) was set at the aperture (end of body chamber) of the ammonoid (Fig. 3E). The body chamber is the final part of the shell that protects the soft parts of the ammonoid (see reconstruction in Fig. 3F). The second landmark (B) was set opposite of the aperture in a way to obtain the longest distance (longitudinal axis, Fig. 4A–C). In cases where the aperture could not be identified, mostly due to bad preservation, points A and B

were nevertheless set but carry less information, i.e., they indicate length but correspond only randomly to the position of the aperture. Data from those latter ammonoids were excluded from analyses at which the aperture direction would be important. The third landmark, needed for defining the orientation of an imaginary sagittal-plane through the ammonoid (Fig. 4D–F), was set at the venter (external position) of the ammonoid, lateral and between points A and B (Fig. 3E and F). The Cartesian coordinates were exported as ASCII-file and imported to Microsoft Excel to calculate the spatial orientation of each ammonoid specimen (Fig. 4 and Table 1).

3.3.2. Spatial orientation parameters computed from landmark coordinates

Trigonometric and vector-based calculations were used to compute the orientation of the diameter (linear between points A and B=a; Fig. 4A–C) as well as of an imaginary sagittal-plane through each ammonoid (triangles in blue, Fig. 4D–F). Therefore the following parameters, comparable to geological features (e.g., Wallbrecher 1978, 1979, 1986; Adler et al., 1982), were calculated from the segmented ammonoids using Microsoft Excel, (Fig. 4 A–F and Table 1):

- (1) Orientation of the linear:
 - a – maximum diameter (Fig. 4A).
 - β – dip of the linear A:B (Fig. 4A).
 - γ – dip direction (Fig. 4B).
 - δ – aperture direction (Fig. 4C).
- (2) Orientation of the imaginary sagittal-plane:
 - ϵ – dip of the plane (Fig. 4D).
 - φ – strike (Fig. 4E).
 - ω – azimuth (Fig. 4F).

The associated equations to each parameter can be gleaned from the corresponding calculation number (Calc. no.) of Table 1. The orientations of the ammonoids were calculated in relation to the grinding sections, thus the z-axis (Fig. 2B). The plane spanned

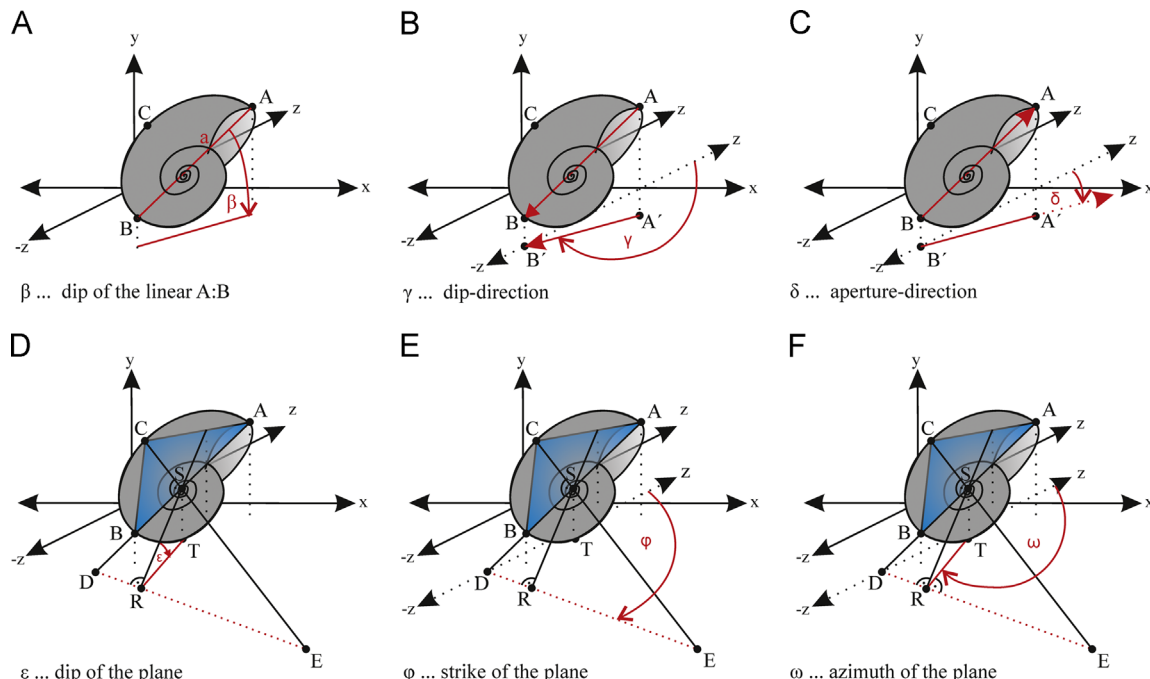


Fig. 4. Explanation of the orientation parameters used for subsequent investigation of the spatial orientation of each ammonoid. (A) Maximum diameter and dip of the linear A:B. (B) Dip-direction. (C) Aperture direction. (D) Dip of the plane (A–B–C). (E) Strike of the plane. (F) Azimuth of the plane.

Table 1

Formulae used for calculating orientation parameters of each ammonoid.

Parameter	Calculation	Calc. no.	Figs.
Computing diameter and dip of the linear A:B (β)			
Diameter (distance A:B)	=Square root $[(A_x - B_x)^2 + (A_y - B_y)^2 + (A_z - B_z)^2]$	1	4A, SF2
Dip A:B (β)	= $\sin^{-1}[\text{abs}(A_y - B_y)/\text{distance A:B}] \times 180/\pi$	2	4A, SF2
Calculation of dip direction (γ) and aperture direction (δ)			
Inner product (0,0,1)	= $A_z - B_z$	3	
Absolute value	= $(A_z - B_z)/\text{square root } [(A_x - B_x)^2 + (A_y - B_y)^2 + (A_z - B_z)^2]$	4	
ρ	= $\cos^{-1}[(A_z - B_z)/\text{square root } ((A_x - B_x)^2 + (A_y - B_y)^2 + (A_z - B_z)^2)] \times 180/\pi$	5	4B, SF2
Dip direction (γ)	=If $A_x > B_x \rightarrow \rho$; if $A_x < B_x \rightarrow 360 - \rho$	6	SF3
Aperture direction (δ)	=If $A_y < B_y \rightarrow \text{aperture direction } (\delta) = \text{dip direction } (\gamma)$ =If $A_y > B_y \rightarrow \delta = 180 + \gamma$	7	4C
Computing coordinates of point S (S_x, S_y, S_z), needed for subsequent calculation of the dip of the plane (ϵ)			
Vector AB	= (x_1, y_1, z_1)	8	SF2
	$x_1 = A_x - B_x$		
	$y_1 = A_y - B_y$		
	$z_1 = A_z - B_z$		
Plane	= $x_1 x + y_1 y + z_1 z = x_1 C_x + y_1 C_y + z_1 C_z$	9	SF2
Straight line	= $(x, y, z) = (A_x, A_y, A_z) + \lambda(x_1, y_1, z_1)$	10	SF2
Straight line inserted in plane	= $x_1(A_x + \lambda x_1) + y_1(A_y + \lambda y_1) + z_1(A_z + \lambda z_1) = x_1 C_x + y_1 C_y + z_1 C_z$	11	SF2
Solving the equation based on λ	$\lambda(x_1^2 + y_1^2 + z_1^2) = x_1(C_x - A_x) + y_1(C_y - A_y) + z_1(C_z - A_z)$ $x_2 = C_x - A_x$ $y_2 = C_y - A_y$ $z_2 = C_z - A_z$ $\Lambda = (x_1 x_2 + y_1 y_2 + z_1 z_2) / (x_1^2 + y_1^2 + z_1^2)$ $\Lambda = [(A_x - B_x)(C_x - A_x) + (A_y - B_y)(C_y - A_y) + (A_z - B_z)(C_z - A_z)] / [(A_x - B_x)^2 + (A_y - B_y)^2 + (A_z - B_z)^2]$	12	SF2
Initiation of Λ into the linear equation	$S_x = A_x + \Lambda(A_x - B_x)$ $S_y = A_y + \Lambda(A_y - B_y)$ $S_z = A_z + \Lambda(A_z - B_z)$	13	SF2
Computing coordinates of points D (D_x, D_y, D_z), E (E_x, E_y, E_z) and T (T_x, T_y, T_z) needed for subsequent calculation of the dip of the plane (ϵ)			
D_x	= $A_x + [(-1 \times A_y) / (A_y - B_y)](A_x - B_x)$	14	SF2
D_y	=0		SF2
D_z	= $A_z + [(-1 \times A_y) / (A_y - B_y)](A_z - B_z)$	15	SF2
E_x	= $C_x + [(-1 \times C_y) / (C_y - S_y)](C_x - S_x)$	16	SF2
E_y	=0		SF2
E_z	= $C_z + [(-1 \times C_y) / (C_y - S_y)](C_z - S_z)$	17	SF2
T_x	= S_x	18	4D, SF2
T_y	=0	19	4D, SF2
T_z	= S_z	20	4D, SF2
Computing distances needed for subsequent calculation of the dip of the plane (ϵ)			
Distance D:E	=square root $[(D_x - E_x)^2 + (D_y - E_y)^2 + (D_z - E_z)^2]$	21	4D, SF2
Distance D:T	=square root $[(D_x - T_x)^2 + (D_y - T_y)^2 + (D_z - T_z)^2]$	22	
Distance E:T	=square root $[(E_x - T_x)^2 + (E_y - T_y)^2 + (E_z - T_z)^2]$	23	
Distance S:T	= S_y		
Distance S:D	=square root $[(D_x - S_x)^2 + (D_y - S_y)^2 + (D_z - S_z)^2]$	24	
Distance S:E	=square root $[(E_x - S_x)^2 + (E_y - S_y)^2 + (E_z - S_z)^2]$	25	
Height R:S (triangle D,E,S)	= $(S:D)(S:E)/(D:E)$	26	
Dip of the plane (ϵ)	= $\sin^{-1}[(S:T) / (\text{height R:S})]$	27	
Calculation of the Strike (ϕ) of the plane			
ρ	= $\cos^{-1}[(D_z - E_z) / \text{square root } ((D_x - E_x)^2 + (D_y - E_y)^2 + (D_z - E_z)^2)] \times 180/\pi$	28	
Strike (ϕ)	=if $D_x > E_x \rightarrow \rho$; if $D_x < E_x \rightarrow 360 - \rho$	29	4E, SF3
Computing coordinates of point R (R_x, R_y, R_z), needed for subsequent calculation of the Azimuth (ω)			
Vector DE	= (x_1, y_1, z_1)	30	SF2
	$x_1 = D_x - E_x$		
	$y_1 = D_y - E_y$		
	$z_1 = D_z - E_z$		
Plane	= $x_1 x + y_1 y + z_1 z = x_1 T_x + y_1 T_y + z_1 T_z$	31	
Straight line	= $(x, y, z) = (D_x, D_y, D_z) + \lambda(x_1, y_1, z_1)$	32	
Straight line inserted in plane	= $x_1(A_x + \lambda x_1) + y_1(A_y + \lambda y_1) + z_1(A_z + \lambda z_1) = x_1 T_x + y_1 T_y + z_1 T_z$	33	
Solving the equation based on λ	$\Lambda(x_1^2 + y_1^2 + z_1^2) = x_1(T_x - D_x) + y_1(T_y - D_y) + z_1(T_z - D_z)$ $x_2 = T_x - D_x$ $y_2 = T_y - D_y$ $z_2 = T_z - D_z$ $\Lambda = (x_1 x_2 + y_1 y_2 + z_1 z_2) / (x_1^2 + y_1^2 + z_1^2)$ $\Lambda = [(A_x - B_x)(C_x - A_x) + (A_y - B_y)(C_y - A_y) + (A_z - B_z)(C_z - A_z)] / [(D_x - E_x)^2 + (D_y - E_y)^2 + (D_z - E_z)^2]$	34	
Initiation of Λ into the linear equation	$R_x = D_x + \Lambda(D_x - E_x)$ $R_y = D_y + \Lambda(D_y - E_y)$ $R_z = D_z + \Lambda(D_z - E_z)$	35	
Azimuth (ω)	If $E_x < D_x, E_z > D_z, T_x > R_x \rightarrow \text{Strike} - 90^\circ$ If $E_x < D_x, E_z > D_z, T_x < R_x \rightarrow \text{Strike} + 90^\circ$ If $E_x > D_x, E_z > D_z, T_x < R_x \rightarrow \text{Strike} + 90^\circ$ If $E_x > D_x, E_z > D_z, T_x > R_x \rightarrow \text{Strike} - 90^\circ$ If $E_x < D_x, E_z < D_z, T_x > R_x \rightarrow \text{Strike} + 90^\circ$	36	4F

Table 1 (continued)

Parameter	Calculation	Calc. no.	Figs.
	If $E_x < D_x$, $E_z < D_z$, $T_x < R_x \rightarrow$ Strike –90°		
	If $E_x > D_x$, $E_z < D_z$, $T_x < R_x \rightarrow$ Strike –90°		
	If $E_x > D_x$, $E_z < D_z$, $T_x > R_x \rightarrow$ Strike –90°		

by the x - and the z -axes indicates the ground plane. The direction of the positive y -axis represents the height from the ground plane (Fig. 2B). For calculating the orientation of the ammonoids as they were deposited in the field, it is necessary to know the deviation of the z -axis from true north, and to add this geographic angle to the calculated geographic parameters (i.e., dip direction, azimuth respectively strike). As dip and azimuth values of the whole bed are 50/075 we add 75° to the calculated aperture direction, dip direction as well as to the calculated azimuth (Fig. 2B).

(1) Orientation of the linear A:B (a).

Maximum diameter of each ammonoid (a).

Definition: The maximum diameter (a) of each ammonoid is represented by the spatial distance between the points A and B (Table 1, Calc. no. 1; Fig. 4A). Associated variables are shown within Supplementary Fig. 2.

Dip of the linear (β).

Definition: The dip (β), or also called the “angle of fall” from the linear (a) represents the angle between the diameter (linear of the landmarks A:B) and the ground plane, spanned by the x - and z -axes (Table 1, Calc. no. 2; Fig. 4A, Supplementary Fig. 2).

Dip direction (γ).

Definition: The dip direction is the geographic orientation towards that the linear A:B is inclined. It is represented by the angle between north (positive z -axis –75°; see Fig. 2B), and the projected linear A:B vectored to A or B respectively, on the ground plane (spanned by the x - and the z -axes). If point B shows a lower y -value (Fig. 4B), the linear A:B is inclined to B and therefore the vector A':B' is directed to point B'. If point A shows a lower y -value, the linear A:B is inclined to A and the vector A':B' is directed to point A' (Table 1, Calc. nos. 3–6; Supplementary Figs. 2 and 3).

Aperture direction (δ).

Definition: The aperture direction is defined as the geographic orientation in which the aperture of the ammonoid is directed (Fig. 4C). It is represented by the angle between north (z axis –75°; Fig. 2B), and the projected linear A:B vectored always to A on the ground plane (Table 1, Calc. no. 7; Fig. 4C).

(2) Orientation of the imaginary sagittal-plane (A–B–C) through the ammonoid.

As already described by Wallbrecher (1986), the orientation of a plane can be defined exactly by two angles. The dip represents the degree of inclination of the plane from the horizontal earth surface. The second angle needed is the azimuth, which is the angular deviation of this declination (dip) from the north (Fig. 4D and F).

Dip of the plane A–B–C (ϵ).

Definition: The dip of the plane, represented by the inclination of the plane from the earth surface, can be defined more precisely as the linear representing the steepest possible angle between the plane (A–B–C) and the ground-plane (spanned by the x - and z -axes) (Fig. 4D). To investigate this linear, the intersection line at which the extended plane (A–B–C to A–C–D–E; see Fig. 4D–F) crosses the ground plane, was constructed and calculated (linear D:E; Fig. 4D). The height (R:S) of the triangle S:D, S:E and D:E, perpendicular to the linear D:E represents the steepest possible linear. Its inclination to the ground floor represents the sought dip of the plane (ϵ ; Table 1; Calc. nos. 8–

27; Fig. 4D, Supplementary Fig. 2).

Strike (ρ).

Definition: The “strike” represents the geographic angular deviation from north (z –75°; Fig. 2B) of the linear at which the extended plane A–B–C intersects with the ground-plane (D:E; Table 1, Calc. no. 29; Fig. 4E; Supplementary Figs. 2 and 3).

Azimuth (ω).

Definition: The azimuth is the geographical direction in which the dip of the plane is inclined. It is the angle between north (z -axis –75°) and the projected linear of the steepest possible linear of the plane (R:S) to the ground plane (Fig. 4F). The azimuth represents the strike ±90° (Table 1, Calc. nos. 30–36; Fig. 4F, Supplementary Fig. 2).

4. Spatial orientation as key to the pleoenvironment

The geographic orientations (cardinal directions) of the ammonoids were analyzed in rose diagrams. The Schmidt net analyses (stereographic projections) were used for combined analyses of geographic orientation and inclination of the ammonoids. These statistical analyses have become standard methods for analyzing spatial orientation of geological features in geoscience and are therefore not explained in detail. Detailed information about these methods can be found in a series of geological literature (e.g., Wallbrecher, 1986; Adler et al., 1982), but also in Mardia and Jupp (2000) which focuses on directional statistics. All analyses and their concluding assumptions were based on the results obtained by the statistical software Fabric8.

4.1. Geographical alignment of the aperture

To investigate the statistical aperture orientation (i.e., direction in the coordinate system), only data from ammonoids with known apertural position ($n=193$) were analyzed. By plotting the aperture direction within a rose diagram a bimodal distribution with 66% preferred orientation, bearing a dominant mean SSE vector (155°), was found (Fig. 5A). With a class-size of 20°, the maximum volume lies within the 160–180° class and represents 18.2%. However, there are two more dominating classes (320–340° and 340–360°) exactly opposite the most dominant class (160–180°), each represented by a volume of 14.9%. Due to this dubious result (almost precise NW–SSE orientation of the apertures, showing a low skewness (–0.37), but a relatively high kurtosis (–42.52; Fig. 5A)), we had to exclude a possible error. For identifying, quantifying and correcting the possible error source, the following test series was carried out (Fig. 5B).

4.1.1. Test series

The aperture of a hypothetical ammonoid, with indicated true aperture direction (blue arrow) was orientated to 21 different directions (0–360°) with periodic displacements of 17° (Fig. 5B). This series of differently orientated ammonoids was copied 12 times and each of them assigned to an artificial ammonoid diameter (1 mm, 3.5 mm, 6 mm, 8.5 mm, 11 mm, 13.5 mm, 16 mm, 18.5 mm, 21 mm, 23.5 mm, 26 mm and 28.5 mm). The resulting sample of 252 ammonoid specimens featuring different diameters and orientations were intersected every 2 mm (Fig. 5B).

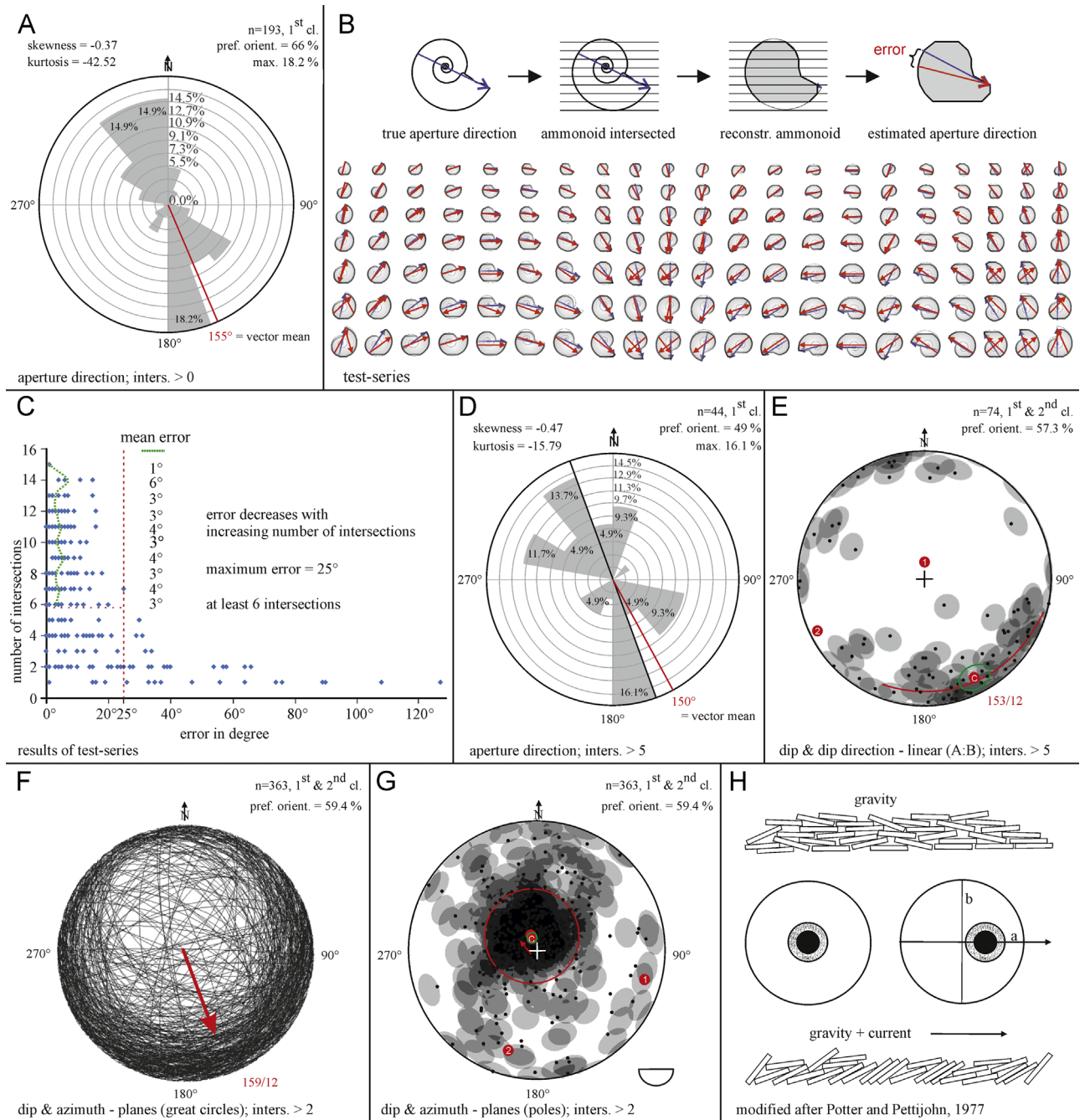


Fig. 5. Results of analyzed spatial shell orientation. (A) Rose diagram showing nearly exact NNW/SSE aperture orientation of all ammonoids at which the aperture could be identified. (B) Example of the test series for calculating the error between estimated- and true- aperture direction. (C) Analysis of test series. (D) Rose diagram showing revised orientation of the aperture direction, only from ammonoids intersected at least 6 times (NW/SE). (E) Results of dip and dip direction of the linear (A:B) analyzed within a Schmidt net plot. (F and G) Results of dip and azimuth of the planes (A-B-C) respectively ammonoids analyzed within a Schmidt net plot. (F) Plot of great circles. (G) Plot of plane-poles. (H) Comparison of the orientation of disks due to gravity respectively gravity plus current action, modified after [Potter and Pettijohn \(1977\)](#).

This setting simulates our grinding approach that in fact eliminates the whole material of the fossilized block while only preserving one snapshot at 2 mm each. Thus, the position of landmarks A-C can, within limits, be wrongly assessed. To learn more about this effect, we studied the possible error between the true- and the estimated aperture-direction (red/blue arrows; Fig. 5B). A simple bivariate plot shows that the error (maximum=127°) decreases with increasing diameter, respectively with increasing number of intersection lines (Fig. 5C). The non-linear distribution suggests a reasonable

cut-off point at 25° (red pointed lines), which means that each ammonoid should be intersected at least six times (Fig. 5C). Hence, for analyzing parameters of the lines (A:B), we used only those ammonoids which were intersected at least six times. For analyzing the orientation of the plane (A-B-C), three intersections were enough because it is reconstructed from three points and therefore the error is significantly lower.

It has to be noted, that the orientation of the intersected 2D ammonoids describes the worst case, a position at which the aperture can hardly be identified. If the ammonoid would be

intersected sagittally (perpendicular to the tested direction of intersection) the error would become much lower.

4.2. Revised aperture direction

The geographic distribution of the aperture direction shows a higher variation (kurtosis = -15.79) by using only ammonoids intersected at least six times ($n=44$). The distribution is unchanged bimodal with an almost similar vector mean at 150° . The maximum class volume (16.1% at $160\text{--}180^\circ$) still plots closely to the south (Fig. 5D). The preferred orientation declines to 49% and changes from NNW-SSE to NW-SE. Furthermore, the opposite dominant class-volume is constricted to the class $320\text{--}340^\circ$, bearing 13.7%, what results in the already mentioned shift from NNW-SSE to NW-SE. Although the skewness changed slightly (-0.47 vs. -0.37), the kurtosis changed from -42.52 to -15.79, due to the higher variation (Fig. 5A,D).

4.3. Dip and dip direction of the linear A:B

Dip and dip direction of the linear (A:B) were analyzed in combination, by using a Schmidt net plot (Fig. 5E). Data from all reconstructed ammonoids intersected at least six times ($n=74$) were included. Identification of the aperture direction is, in this case, of no importance. Each data point represents one dip in combination with its dip direction. Most points are plotted at the outer edge of the circle, which indicates a relatively slight dip. Points close to the center would reflect a steep dip. The geographic distribution can be gleaned from this plot in the same way as from rose diagrams. Points near the top (N) indicated a northern direction, etc. The plot shows a preferred orientation of 57.3% of the linears (length of vector sum; 100% = parallel orientation), which are slightly inclined (12°) toward SE (153°). The true center of gravity (comparable to the mean within the linear statistics) plots with a significance of 0.05 within the cone of confidence (8.6° ; Fig. 5E green circle) around the center of gravity ($153/12$).

4.4. Dip and azimuth of the plane A-B-C

Dip and azimuth of the plane (A-B-C) were analyzed in the same way as dip and dip direction of the linear (A:B), with the difference that the data were taken from ammonoids intersected at least three times ($n=363$). The identification of the aperture direction is of no importance here as well. Fig. 5F shows a stereographic projection of great circles. Each great circle represents the geographic orientation (dip and azimuth) of one plane (respectively ammonoid). Like for the data points of the linears, great circles plotting close to the center indicate a steep inclination, whilst great circles near the periphery indicate a slight inclination. The data plot (Fig. 5F) therefore shows that 59.4% (preferred orientation, length of vector sum) are slightly inclined (12°) toward SE (159°). Another possibility for analyzing planes within a stereographic graph is by plotting their plane-poles (orthogonal axis through the center of gravity of the triangles; Fig. 5G). In the case of analyzing the poles, data points indicate the projection of the orthogonal axis of the planes. Points plotting close to the center indicate only a slight inclination of the planes respectively of the ammonoids. The geographic distribution can be interpreted in the same way as from the plots of the linears. While the planes are inclined toward SE (see great circles, Fig. 5F), their plane poles plot toward NW due to the fact that the plane poles are orthogonal to the planes (Fig. 5G). The preferred orientation of the plane-poles (vector sum = 59.4%) plot near to, but not in the center (white cross), toward NW. The true center of gravity of the planes (comparable to the true mean within the linear statistics) plots with a significance of 0.05 within the cone of confidence

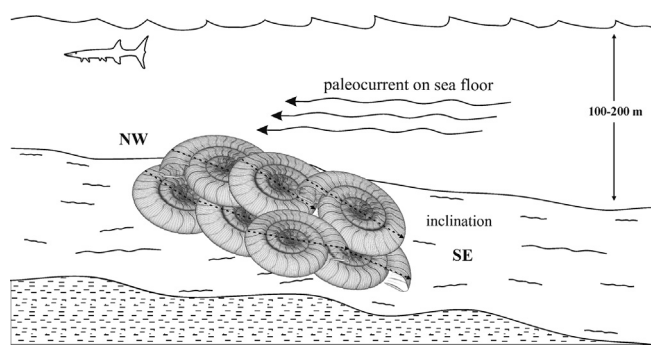


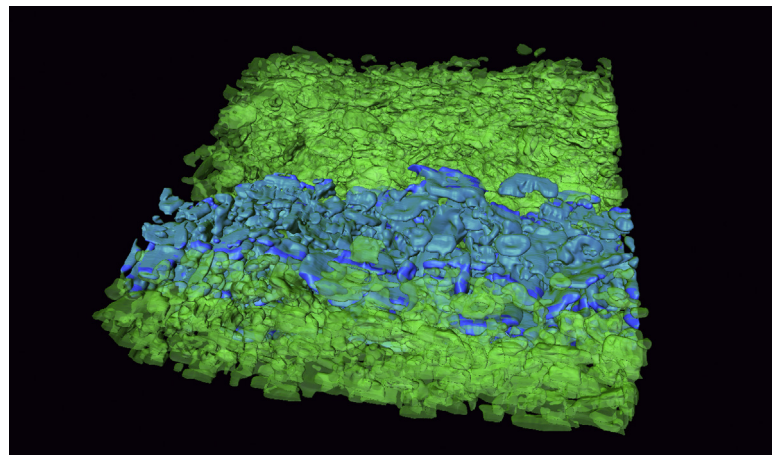
Fig. 6. Reconstructed current- and environmental conditions of the primary ammonoid-deposition on the sea floor. Ammonoid-grids were modeled by Michael Klein (7Reasons Media Corporation).

(3.7°) around the center of gravity ($159/12$; Fig. 5G). This indicates a slight inclination of the planes (respectively ammonoids) toward SE (Fig. 5F and G). Potter and Pettijohn (1977), for comparison, described the orientation of disks for gravity as well as for gravity plus current actions by the use of stereographic projections (Fig. 5H). The imbrication of such disks would result in a shift of the center of gravity from the center of the Schmidt net plot in the down-current direction, as a result of tangential transport (Sander, 1930; Potter and Pettijohn, 1977). By comparing these conclusions to the slightly NW shifted maximum concentration of the plane poles herein, the latter can be interpreted as a smooth but significant movement of the ammonoids, or respectively as a current direction, oriented toward NW (Fig. 6).

5. Discussion

As mentioned in Section 1.2, the investigation of fossil orientation from bedding planes for estimating ancient paleocurrents has been conducted in numerous studies (e.g., Hall, 1843; King, 1948; Kidwell et al., 1986). However, the majority of these studies deal with elongated fossils (e.g., belemnites, cephalopods with orthoconic shells and gastropods, etc.), excluding planispirally coiled (flat to disk-shaped) morphologies (e.g., shells of ectocoeliate cephalopods such as ammonoids). Brenner (1976), and more recently Wani (2006), claimed that the body chambers of empty ammonoid shells can be used as current indicators, orientated with their aperture downstream. Futterer (1982) reported that planispiral gastropod shells (e.g., *Planorbina* sp.) manifested their stable position with the aperture downstream. Lukeneder (2005) interpreted planispiral and elongated ammonoids, orientated on the sea floor of an Early Cretaceous section in Upper Austria, as bottom current induced. Moreover, Wendt (1995) compared the orientation of goniatictic (planispiral-coiled) cephalopods and orthoconic cephalopods (elongated shells). He reported that the orientations of goniaticites (disk-shaped shells) in some cases appear nearly randomly. Therefore, he suggested caution for interpreting paleocurrents from the aperture direction of coiled cephalopods. However, none of these studies interpreted planispiral-coiled cephalopods with respect to the orientation of their disk-like morphologies. As shown in this study, the orientation of these forms can simply be interpreted like the orientation of disks, compared to Sander's approach (1930) (Fig. 5H) on the alignment-behavior of disk-like particles (Potter and Pettijohn, 1977).

Additionally, conventional studies of fossil-orientation-measurements, predominantly deal with the two-dimensional geographic orientation of a certain axis of the fossil, analyzed within rose diagrams. Azimuth directions of fossils have been measured for tentaculite shells of Bohemia (Hladil et al., 1996), or for nerineoid shell beds (Cataldo et al., 2013), though disregarding



Video S1. A video clip is available online. Supplementary material related to this article can be found online at <http://dx.doi.org/10.1016/j.cageo.2013.11.008>.

stereographic plots for a combined interpretation of dip and azimuth. Numerous studies on sedimentology dealt with the imbrication of pebbles as proxies for determination of paleocurrents (e.g., Sengupta, 1966; Trendell et al., 2013; Karátson et al., 2002). White (1952) investigated the flow direction of a depositing stream from the Houghton conglomerate with respect to the initial imbrication of pebbles. Even more than a decade earlier, Krumbein (1940) used imbricated pebbles to determine the transport direction of California flood gravels. More recent studies automated the analysis of imbrication and flow direction by using Laser-Scan data (Millane et al., 2006). We applied Sander's (1930) approach of the orientation of disk-like particles to the disk-shaped ammonoids (i.e., *Kasimlarceitites*). Both results, the orientation of the aperture, as well as the orientation of the estimated sagittal-plane through the ammonoids (dip and azimuth), indicate a movement of the ammonoids or respectively a current direction toward NW (Fig. 6). It shows that the combined interpretation of dip and azimuth of disk-shaped fossils represents a significant approach for interpreting sea floor paleocurrents.

Hitherto, the investigation of fossil-orientation was only used for the topmost surface of fossil mass occurrences, deposited directly on the sea floor. Due to the fast development of virtual methods (e.g., macro-CT, μ -CT, nano-CT, etc.) it became possible, to investigate the interior orientation of such fossil mass occurrences in three-dimensional detail. Although, a series of paleontological studies deal with 3D-visualization of fossil-elements, no mass occurrence has previously been reconstructed three dimensionally for investigating their interior orientation. This study illustrates an interdisciplinary approach of virtual reconstruction, analyses and interpretation of the interior orientation of an ammonoid mass occurrence. The method established herein produces clear and consistent results using planispirally coiled ammonoid shells – fossils, that so far would have been used only with caution for depositional interpretations. This method can be applied to any kind of fossil mass occurrence, or even other abundant organic elements and particles, to examine their orientation and depositional conditions to conclude on their paleoenvironment, particularly on paleocurrents.

6. Conclusions

In our study, we introduce a new method, which combines digital fossil-segmentation, subsequent 3D-reconstruction and calculation of spatial ammonoid-orientation, performed on a Triassic ammonoid mass occurrence, deposited within a limestone layer, at Aşağıyaylabel (Taurus Mountains, Southern Turkey). Since

computed tomography could not be used for digitization because of insufficient density contrast, the classic method of serial grinding was applied. A block, $150 \times 45 \times 140 \text{ mm}^3$, of the limestone layer was ground and 70 slices with a distance of 2 mm were scanned in longitudinal direction (from 1A to 1C; Fig. 2B). The semi-automatic region growing tool of Amira was applied for segmentation and 3D-reconstruction of the ammonoids. Six orientation parameters, already known from geological features, were calculated from these ammonoids. The use of the Cartesian coordinates of three different landmarks, placed on three particular points of each ammonoid, made it possible to calculate the orientation parameters and therefore the spatial orientation of 675 segmented ammonoids from a 26 mm part of the whole block. The analyses, via rose diagrams and Schmidt net plots, show a general NW/SE orientation of the aperture direction of the ammonoids, as well as a slightly SE inclination of the whole ammonoids, indicating a slight but significant sediment movement or even possible a current direction toward NW.

Using this method in an ongoing study, the orientation of all ammonoids from the whole block will be investigated. The statistical orientation of all ammonoids from the mass occurrence, combined with additional 2D-reconstructions and facies-analyses of the limestone-layer, should lead to more detailed conclusions about the depositional conditions of the ammonoid mass occurrence. The newly established method can be used as template for measuring spatial orientations on all kinds of fossil mass occurrences or other geological objects. A new animation clip (see **Supplementary material**) explains all steps, from segmentation, over surface-reconstruction to landmark-positioning, within the software package Amira, hence helping to apply this method to comparable material and scientific fields. Video 1

Acknowledgments

This study was funded by the Austrian Science Fund (FWF, P 22109-B17). The authors thank Yeşim İslamoğlu (Ankara) and the General Directorate of Mineral Research and Exploration (Ankara) for the digging permission and the organization of two field trips. We are grateful to Mathias Harzhauser (Vienna), Philipp Strauss (Vienna) and Leopold Krystyn (Vienna) for providing material from previous field trips. Special thanks go to Franz Topka (Vienna) for his help during field trips and for grinding the reference-block. The authors thank Robert Marschallinger (Salzburg) and Christian Klug (Zurich) for constructive reviews of the manuscript. We thank Michael Schwaiger (Linz) and Martin Mayrhofer (Waldegg) for fruitful discussions concerning mathematical questions as well as

Ulrike Exner (Vienna) for the possibility of using the software package Amira on her high-capacity PC. Andreas Kroh (Vienna) helped with useful advices concerning the digitization of the slices. Eckart Wallbrecher (Graz) is thanked for advice on statistical questions concerning the stereographic projection. Additionally, we acknowledge Simon Schneider (Cambridge) for his support in collecting hardly obtainable literature. The authors thank Maarten Voorn (Vienna) for the introduction to the software package Avizo as well as Martin Dockner (Vienna) for hardware-advises. Michael Klein (Vienna) from 7reasons Media Corporation is thanked for the help with the final animation clip-rendering.

Appendix. Supplementary material

Supplementary data associated with this article can be found in the online version at <http://dx.doi.org/10.1016/j.cageo.2013.11.008>.

References

- Adler, R., Fenchel, W., Pilger, A., 1982. Statistische Methoden in der Tektonik II. Clausthaler Tektonische Hefte, vol. 4; 1–89.
- Brenner, K., 1976. Ammoniten-Gehäuse als Anzeiger von Palaeo-Strömungen. Neues Jahrbuch für Geologie und Paläontologie, Abhandlungen, vol. 151; 101–118.
- Briguglio, A., Metcher, B., Hohenegger, J., 2011. Growth rate biometric quantification by x-ray microtomography on larger benthic foraminifera: three-dimensional measurements push nummulitids onto the fourth dimension. *Turk. J. Earth Sci.* 20, 683–699.
- Camp, C.L., Hanna, G.D., 1937. Methods in Paleontology. University of California Press, Berkley, pp. 53–55.
- Cataldo, C.S., Lazo, D.G., Tunik, M.A., Aguirre-Urreta, M.B., 2013. Taphonomy and palaeoecology of Hauterivian-Barremian nerineoid shell beds from the Neuquén Basin, west-central Argentina. *Lethaia* 46, 114–126.
- Conroy, G.C., Vannier, M.W., 1984. Noninvasive three-dimensional computer imaging of matrix-filled fossil skulls by high-resolution computed tomography. *Science* 226, 456–458.
- Dercourt, J., Ricou, L.E., Vrielynck, B., 1993. Atlas Tethys Palaeoenvironmental Maps. Gauthier-Villars, Paris p. 307.
- Dercourt, J., Gaetani, M., Vrielynck, B., Barrier, E., Bijou-Duval, B., Brunet, M.F., Cadet, J.P., Crasquin, S., Sandulescu, M. (Eds.), 2000. Atlas Peri-Tethys – Palaeogeographical Maps. Commission of the Geological Map of the World, Paris.
- Dockner, M., 2006. Comparison of *Crocuta crocuta* and *Crocuta crocuta spelaea* through computer tomography (Unpublished Diploma thesis). University of Vienna, Vienna, 68pp.
- Flügel, E., 2004. Microfacies of Carbonate Rocks. Analysis, Interpretation and Application. Springer, Berlin Heidelberg New York p. 182.
- Fourie, S., 1974. The cranial morphology of *Thrinaxodon liorhinus* Seeley. *Ann. S. Afr. Mus.* 65, 337–400.
- Futterer, E., 1982. Experiments on the distinction of wave and current influenced shell accumulations. In: Einsele, G., Seilacher, A. (Eds.), Cyclic and Event Stratification, pp. 175–179.
- Garwood, R.G., Imran, A.R., Sutton, M.D., 2010. From clergymen to computers – the advent of virtual palaeontology. *Geol. Today* 26 (3), 96–100.
- Gindl, A., 2000. Paläökologie Triassischer Ammonitenfaunen des Taurusgebirges (Türkei) (Unpublished Diploma thesis). University of Vienna, 80pp.
- Hall, J., 1843. Geology of New York, Part IV. Carroll and Cook, Albany p. 683.
- Hladil, J., Čejchan, P., Gabašová, A., Tděáboršký, Z., Hladíková, J., 1996. Sedimentology and orientation of tentaculite shells in turbidite lime mudstone to packstone: Lower Devonian, Barrandian, Bohemia. *J. Sediment. Res.* 66; , pp. 888–899.
- Karátson, D., Szánó, O., Telbisz, T., 2002. Preferred clast orientation in vulcaniclastic mass-flow deposits: Application of a new photo-statistical method. *J. Sediment. Res.* 72 (6), 823–835.
- Kelling, G., Moshrif, M.A., 1977. The orientation of fossil bivalves in a pene-littoral sequence (the Rhaetian of South Wales). *J. Sediment. Petrol.* 47 (3), 1342–1346.
- Ketcham, R.A., Carlson, W.D., 2001. Acquisition, optimization and interpretation of X-ray computed tomographic imagery: applications to the geosciences. *Comput. Geosci.* 27, 381–400.
- Kidwell, S.M., Fürsich, F.T., Aigner, T., 1986. Conceptual framework for the analysis and classification of fossil concentrations. *Palaios* 1, 228–238.
- King, P.B., 1948. Geology of the Southern Guadalupe Mountains, Texas. United States Geological Survey Professional Paper 215. pp. 1–183.
- Koslowski, R., 1932. Sur un procédé simple et précis d'effectuer les coupes sérielles des fossiles. *Palaontol. Z.* 13, 316–318.
- Krumbein, W.C., 1940. Flood gravels of San Gabriel Canyon. *Geol. Soc. Am. Bull.* 51, 639–676.
- Kruta, I., Landman, N., Rouget, I., Cecca, F., Tafforeau, P., 2011. The role of ammonites in the Mesozoic Marine Food Web revealed by Jaw Preservation. *Science* 331/6013, 70–72.
- Lukeneder, A., 2005. Taphonomy and Stratigraphy of Early Cretaceous ammonoid mass occurrences (Late Valanginian; Northern Calcareous Alps; Upper Austria). *Austrian J. Earth Sci.* 98, 34–51.
- Lukeneder, A., 2012. Computed 3D visualization of an extinct cephalopod using computer tomographs. *Comput. Geosci.* 45, 68–74.
- Lukeneder, S., Lukeneder, A., 2011. Methods in 3D modelling of triassic ammonites from Turkey (Taurus, FWF P22109-B17). In: Marschallinger, R., Zobl, F. (Eds.), Mathematical Geosciences at the Crossroads of Theory and Practice, Proceedings IAMG 2011 Conference, pp. 497–507.
- Lukeneder, S., Lukeneder, A., Harzhauser, M., Islamoglu, Y., Krystyn, L., Lein, R., 2012. A delayed carbonate factory breakdown during the Tethyan-wide Carnian Pluvial Episode along the Cimmerian terranes (Taurus, Turkey). *Facies* 58, 279–296.
- Lukeneder, S., Lukeneder, A., 2013. A new ammonoid fauna from the Carnian (Upper Triassic) Kasimlar Formation of the Taurus Mountains (Anatolia, Turkey). *Palaontology*. (in press).
- Malcom, J.H., Jones, B.J., 2001. Contour correspondence for serial section reconstruction: complex scenarios in paleontology. *Comput. Geosci.* 27, 427–440.
- Mardia, K.V., Jupp, P.E., 2000. Directional Statistics. Wiley, Chister, New York, Weinheim, Brisbane, Singapore, Toronto p. 430.
- Marschallinger, R., 2001. Three-dimensional reconstruction and visualization of geological materials with IDL – examples and source code. *Comput. Geosci.* 27, 419–426.
- Marschallinger, R., Hofmann, P., Daxner-Höck, G., Ketcham, R.A., 2011. Solid modeling of fossil small mammal teeth. *Comput. Geosci.* 37, 1364–1371.
- Mayrhofer, S., Lukeneder, A., 2011. 3D modelling in palaeontology – a case study on the Triassic ammonite *Orthocerites* (Carnian, Taurus, Turkey). *Geophys. Res. Abstr.* 13. (EGU2011–1833).
- Millane, R.P., Weir, M.I., Smart, G.M., 2006. Automated analysis of imbrication and flow direction in alluvial sediments using laser-scan data. *J. Sediment. Res.* 76, 1049–1055.
- Olivero, E.B., 2007. Taphonomy of ammonites from the Santonian-Lower Campanian Santa Marta Formation, Antarctica: Sedimentological controls on vertically embedded ammonites. *Palaios* 22, 586–597.
- Potter, P.E., Pettijohn, F.J., 1977. Paleocurrents and Basin Analysis, 2nd ed. Springer-Verlag, Berlin, Heidelberg, New York p. 425.
- Sander, B., 1930. Gefügekunde der Gesteine. Springer-Verlag, Wien p. 352.
- Scotese, C.R., 1998. Quicktime Computer Animations. PALEOMAP Project. Department of Geology, University of Texas at Arlington.
- Scotese, C.R., 2001. Paleomap Project. [\(http://www.scotese.com/\)](http://www.scotese.com/) (accessed July 2001).
- Scotese, C.R., Gahagan, L.M., Larson, R.L., 1989. Plate tectonic reconstructions of the Cretaceous and Cenozoic ocean basins. In: Scotese, C.R., Sager, W.W. (Eds.), Mesozoic and Cenozoic plate reconstructions. Elsevier, Amsterdam, pp. 27–48.
- Seilacher, A., 1959. Fossilien als Strömungs-Anzeiger. *Aus der Heim.* 67, 170–177.
- Seilacher, A., 1960. Strömungsanzeichen im Hunsrückschiefer. *Notizblatt des Hessischen Landesamtes für Bodenforschung*, vol. 88; 88–106.
- Seilacher, A., 1971. Preservational history of ceratite shells. *Palaeontology* 14 (1), 16–21.
- Sengör, A.M.C., Yilmaz, Y., Sungurlu, O., 1984. Tectonics of the Mediterranean Cimmerids: Nature and Evolution of the Western Termination of Paleo-Tethys. Geological Society of London Special Publications. vol. 17, pp. 77–112.
- Sengupta, S., 1966. Studies on orientation and imbrication of pebbles with respect to cross-stratification. *J. Sediment. Petrol.* 36 (2), 362–369.
- Simpson, G.G., 1933. A simplified serial sectioning technique for the study of fossils. *Am. Mus. Novit.* 634, 1–6.
- Sollas, W.J., 1903. A method for investigation of fossils by serial sections. *Philos. Trans. R. Soc. B* 196, 259–265.
- Spinsby, J., Friedrich, H., Buseck, P.R., 2008. Volume and surface-area measurements using tomography, with an example from the Brenham pallasite meteorite. *Comput. Geosci.* 34, 1–7.
- Stampfli, G.M., Borel, G.D., 2002. A plate tectonic model for the Paleozoic and Mesozoic constrained by dynamic plate boundaries and restored synthetic oceanic isochrons. *Earth Planet. Sci. Lett.* 196, 17–33.
- Stampfli, G.M., Borel, G.D., Marchant, R., Mosar, J., 2002. Western Alps geological constraints on western Tethyan reconstructions. *J. Virtual Explor.* 8, 77–106.
- Stensiö, E.A., 1927. The Downtonian and Devonian Vertebrates of Spitsbergen, Pt. I. Family Cephalaspidae. *Skrifter om Svalbard og Nordishavet*, 12; 1–391.
- Sutton, M.D., 2008. Tomographic techniques for the study of exceptionally preserved fossils. *Proc. R. Soc. B* 275, 1587–1593.
- Trendell, A.M., Atchley, S.C., Nordt, L.C., 2013. Facies analysis of a probable large-fluvial-fan depositional system: The Upper Triassic Chinle Formation at Petrified Forest National Park, Arizona. *U.S.A. J. Sediment. Res.* 83, 873–895.
- VanderHoof, V.L., 1931. *Borophagus littoralis* From the Marine Tertiary of California. University of California Publications, Bulletin Department of Geological Science. vol. 21, pp. 15–24.
- Vasiľkova, J., Lukševičs, E., Stinkulis, G., Zupiņš, I., 2012. Taphonomy of the vertebrate bone beds from the Klūnas fossil site, Upper Devonian Tervete Formation of Latvia. *Est. J. Earth Sci.* 61, 105–119.
- Wallbrecher, E., 1978. Ein Cluster-Verfahren zur richtungsstatistischen Analyse tektonischer Daten. *Geol. Rundsch.* 67, 840–857.
- Wallbrecher, E., 1979. Methods for a quantitative comparison of orientation data using vectorstatistics and eigenvalue analysis with special reference to degrees of preferred orientation and distribution shapes. *N. Jahrb. Geol. Paläontol. Abhandlungen* 159, 113–149.

- Wallbrecher, E., 1986. Tektonische und Gefügeanalytische Arbeitsweisen. Ferdinand Enke Verlag, Stuttgart p. 244.
- Wani, R., 2006. Planispiral Cephalopod Shells as a sensitive indicator of modern and ancient bottom currents: new data from flow experiments with modern *Nautilus pompilius*. *Palaios* 21, 289–297.
- Wani, R., 2007. How to recognize *in situ* fossil cephalopods: evidence from experiments with modern *Nautilus*. *Lethaia* 40, 305–311.
- Weber, G.W., Bookstein, F.L., 2011. Virtual Anthropology – A Guide to a New Interdisciplinary Field. Springer Verlag, Wien, New York p. 423.
- Wendt, J., 1995. Shell directions as a tool in palaeocurrent analysis. *Sediment. Geol.* 95, 161–186.
- Wendt, J., Aigner, T., Neugebauer, J., 1984. Cephalopod limestone deposition on a shallow pelagic ridge: the Tafilalt Platform (upper Devonian, eastern Anti-Atlas, Morocco). *Sedimentology* 31, 601–625.
- White, W.S., 1952. Imbrication and initial dip in a keweenawan conglomerate bed. *J. Sediment. Petrol.* 22, 189–199.